THE INFLUENCE OF THE THERMAL TREATMENT ON LUMINESCENCE PROPERTIES OF ZnO

O. OPREA, O. R. VASILE, G. VOICU[*], E. ANDRONESCU
University Politehnica of Bucharest, Faculty of Applied Chemistry and Materials Science, Romania

As one of the most suitable materials with size- and dimensionality-dependent functional properties, wide bandgap semiconducting ZnO nanostructures have attracted many researchers in recent years. For example, ZnO has been assembled into nanometer-scale visible-light-blind ultraviolet (UV) light sensors with high sensitivity and selectivity, in addition to other applications such as field emitters and lasers.In this paper nanocrystalline ZnO particles were prepared from n-buthanol solution of zinc acetate dihydrate without using base, through a colloid process carried out at refluxing temperature of 118°C. The ZnO nanopowder obtained was characterised by means of XRD, TEM, TG-DSC, UV-Vis, FTIR and fluorescence spectra. The influence of the thermal treatment applied after synthesis on luminescence properties was monitored. We found that there is a clear correlation between the annealing temperature and the ratio of the intensities of the near band-edge and green emissions.

1. Introduction

Semiconductor nanoparticles have attracted interests of many academic and industrial researchers because of their unusual optoelectronic properties [1-4]. Nanosized ZnO can be utilized in electrochemical fields including chemical sensors [5], photocatalysts [6, 7], thin films [8, 9], dye-sensitized solar cells [10] and in various optoelectronic devices as well as in spintronics [11].

ZnO is a direct band gap semiconductor with a band gap of 3.37 eV having an excitonic binding energy of 60 meV. The literature is abundant in reports of ZnO photoluminescence. The photoluminescence spectra of ZnO powders usually presents two emission peaks in the UV and visible ranges [12], the relative intensity of which strongly depended on O_2 pressure used during the synthesis process [13]. These luminescence effects have been assigned to electronic transitions involving the conduction band, the valence band, and various intrinsic or extrinsic defect levels lying within the band gap.

A variety of structural defects may exist in the ZnO nanoparticles, which will influence the electronic and optoelectronic properties. The intrinsic defects commonly found in ZnO are zinc interstitials (Zn_i), zinc vacancies (V_{Zn}), oxygen interstitials (O_i), oxygen vacancies (V_O), oxygen antisites (O_{Zn}), and zinc antisites (Zn_O). A detailed description about these defects has been reported by Kohan *et al* [14].

The UV emission corresponds to the near band edge (NBE) emission (is due to the radiative annihilation of excitons) and the visible emission is commonly referred to as a deep-level or trap-state emission [15]. The relative strength of NBE to deep level defect emissions exhibits a dramatic threshold dependence on surface roughness. Surface optical emission efficiency increases

---

*Corresponding author: getav2001@yahoo.co.uk

over tenfold as roughness decreases to unit cell dimensions, highlighting the coupled role of surface morphology and near-surface defects for high efficiency ZnO emitters [16].

Contradictory results regarding the effect of annealing on the luminescence property of ZnO have been reported in literature. In some experiments [17-21], oxygen annealing has enhanced the intensity of the visible luminescence band and has reduced the intensity of the NBE emission band, while in some other reports the opposite behaviour was observed [22-26]. It was also found that the change in relative intensities of the visible and NBE emission bands depends on the annealing temperature [25, 27, 28].

In this study, nanocrystalline ZnO particles were successfully prepared by modifying our previous method [29]. Controlled hydrolysis of zinc acetate under moderate conditions such as neutral solutions, low temperature, and ambient atmosphere, without using any alkaline solution has led to polyhedral ~ 20nm pure ZnO nanoparticles. The ZnO powder was annealed for 2 hours at temperatures ranged from 300 to 900°C.

The characterization of the nanoparticles included X-ray diffraction, TEM and HRTEM, FTIR, UV-Vis and PL spectra.

Unlike the previous reports, the luminescence of our ZnO nanoparticles shows a strong dependence of post-synthesis thermal treatment, both blue-green and NBE emission bands increasing in intensity.

2. Experimental details

2.1 Experimental procedure

Zinc acetate dihydrate, $Zn(Ac)_2 \cdot 2H_2O$, with 99.9% purity was obtained from Merck. The n-buthanol was used as received from Sigma without further purification.

ZnO synthesis

2.1940g (0.01 moles) $Zn(CH_3COO)_2$ $2H_2O$ were added in 50 mL n-buthanol. The solution was then heated for 24h at reflux (118°C). The white colloidal precipitate formed was then separated by centrifugation at 12.000 rpm and washed several times with methanol. The white powder was dried at 105°C for 30 min in the ambient atmosphere.

Samples from the powder were placed in open crucible and heated with a 10K/min ramp, in the normal atmosphere, to 300, 500, 700 and 900°C, with an annealing time of 2 hrs.

2.2. Experimental techniques

a) Electron Microscope Images. The transmission electron images were obtained on finely powdered samples using a Tecnai^{TM} G^2 F30 S-TWIN high resolution transmission electron microscope from FEI, equipped with STEM/HAADF detector, EDX (Energy dispersive X-ray Analysis) and EFTEM - EELS (Electron energy loss spectroscopy) operated at an acceleration voltage of 300 KV obtained from a Shottky Field emitter with a TEM point resolution of 2 Å and line resolution of 1.02 Å.

b) X-ray Diffraction. X-ray powder diffraction patterns were obtained with a Shimadzu XRD6000 diffractometer, using Cu Kα (1.5406 Å) radiation operating with 30 mA and 40 kV in the 2θ range 10–70°. A scan rate of 1° min^{-1} was employed.

c) Infrared Spectroscopy. The Fourier transform infrared (FTIR) spectra were recorded using the KBr pellet technique on a Bruker Tensor 27 spectrometer in the 4000–400 cm^{-1} frequency range. A total of 30 scans and a resolution of 1 cm^{-1} were employed in getting the spectra.

d) Thermal analysis. Thermal behaviour of the ZnO nanopowder was followed by TG-DSC with a Netzsch TG 449C STA Jupiter. Sample was placed in alumina crucible and heated with 10K·min^{-1} from room temperature to 900°C, under the flow of 10 mL min^{-1} dried air.

e) Photoluminescence spectra. Photoluminescence spectra (PL) were measured with a Perkin Elmer P55 spectrometer using a Xe lamp as a UV light source at ambient temperature, in the range 200-800 nm, with all the samples in solid state. The measurements were made with scan

speed of 200 nm·min^{-1}, slit of 10 nm, and cut-off filter of 1%. An excitation wavelength of 320 nm was used.

f) Diffuse reflectance spectra measurements were made with a JASCO V560 spectrophotometer with solid sample accessory, in the domain 200-850nm, with a speed of 200nm·min^{-1}.

3. Results and discussions

In order to obtain a single-phase compound, the purity of the final product was monitored by TG-DSC analysis and FTIR spectroscopy. Figure 1 shows the FTIR spectra for the obtained ZnO powder (a) and for ZnO powder annealed at 900°C, for 2 hours (b).

For the ZnO powder obtained by this method, absorption bands near 3400 cm^{-1} were attributed to O-H stretching vibration, coming from the surface OH groups and the 1634 cm^{-1} corresponds to water molecules adsorbed on the ZnO nanoparticle's surface.
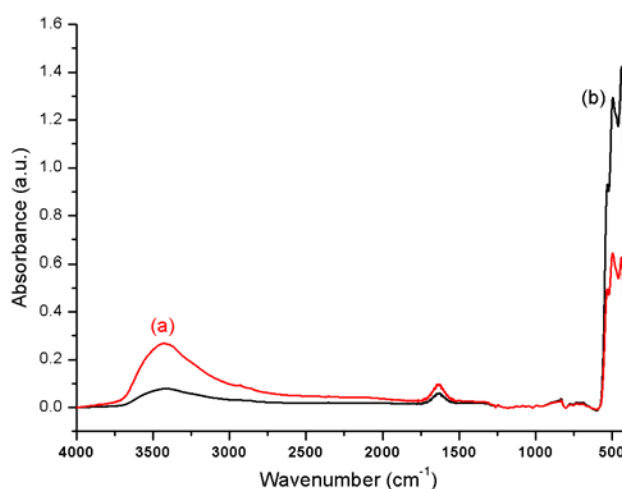

Fig. 1. The FTIR spectra for the obtained ZnO powder (a) and for ZnO powder annealed at 900°C, for 2 hours (b).

Even if the synthesis is carried out in an alcoholic solution, the crystallization water molecules plays an essential role in the reaction mechanism, so is no surprise to find some of them still attached to the nanoparticle's surface. Moreover, the handling of the nanopowder was done in the ambient atmosphere so there is a possibility that some water molecules to come from the air also.

Another two strong absorption bands were observed at 439 and 504 cm^{-1}. The band at 504 cm^{-1} may be associated with oxygen deficiency and/or oxygen vacancy defect complex in ZnO [30]. Changes of oxygen composition can be evaluated also indirectly by variation of intensity of the spectroscopic band at 439 cm^{-1} because this mode involves vibrations of only the oxygen sublattice [31, 32].

The FTIR spectra recorded for ZnO powder annealed at 900°C, for 2 hours, presents same absorption bands, but with different intensities. The lower relative intensity observed for the 3400 cm^{-1} bands (compared with Zn-O characteristic bands) was attributed to the fact that majority of the OH- groups and surface adsorbed water molecules, were removed by the thermal treatment. The higher relative intensity of 439 and 504 cm^{-1} band may indicate an increase of oxygen defects on the surface of nanoparticles. As air or oxygen annealing of ZnO usually diminishes the Vo defect density, but also increase the number of O_i type defects, we correlate the intensity of these bands with the number of O_i type defects. This increase of O_i type defects should translate into an enhanced green emission in PL spectra.

The thermal analysis (figure 2) demonstrated also the purity of ZnO nanoparticles obtained by this method. Virtually no mass loss was recorded between room temperature and 900°C.
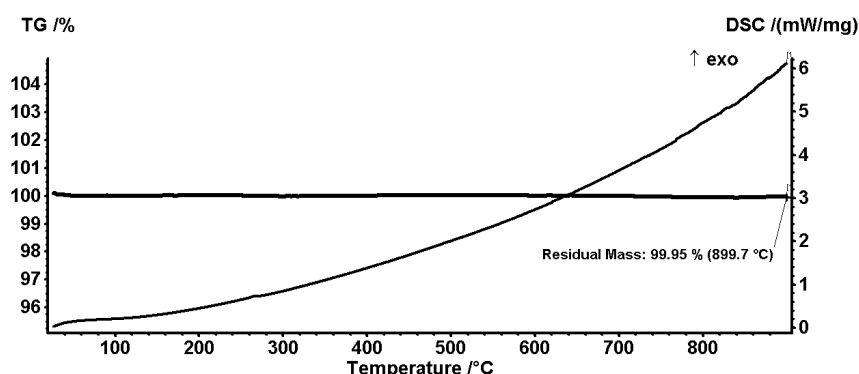
Fig. 2. TG-DTG curves for ZnO powder

The crystalline phase formation was investigated by X-ray diffraction. The XRD data presented in figure 3 demonstrate the formation of ZnO as final product. All patterns can be indexed to a hexagonal wurtzite structure, ASTM 80-0075. The lattice constant calculated for ZnO as obtained are a = b = 3:244Å, c = 5:210Å.

The crystallite size of the samples can be estimated from the Scherrer equation, $D = 0.89 \cdot \lambda / \beta \cdot \cos\Theta$, where D is the average grain size, λ is the X-ray wavelength (0.15405 nm), Θ and β are the diffraction angle and FWHM of an observed peak, respectively. The strongest peak (101) at $2\Theta = 36.21^{o}$ was used to calculate the average crystallite size (D) of ZnO particles. The estimated average crystallite size increases from 14nm to about 21nm when increasing the thermal treatment temperature up to $900^{o}C$.

It is also found that the relative intensity of all peaks increases with increasing of annealing temperature. The strongest increase is observed for the (1 0 1) peak. This indicates a preferential orientation along the [101] direction. The exception from this variation is the decreasing intensity of the (0 0 2) peak between 700 and $900^{o}C$, probably due to some physical processes (e.g. coalescence of the nanoparticles). It should be mentioned that the most possible growth direction in ZnO is the [001] direction due to the lowest surface energy [33].
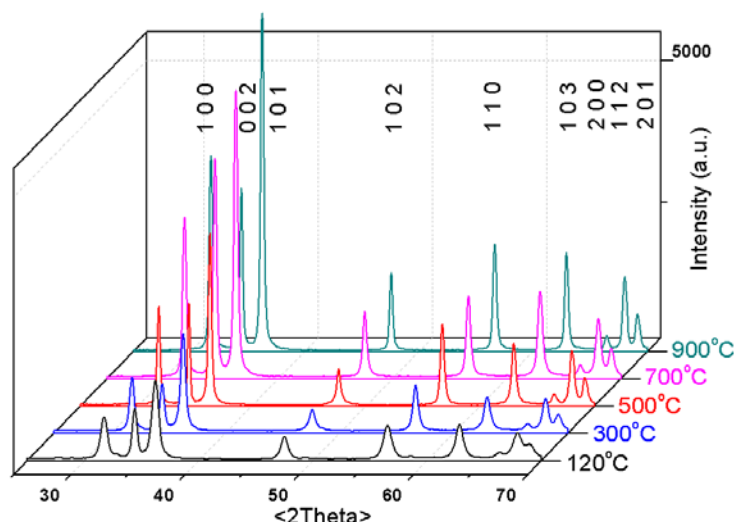

Fig. 3. XRD patterns of ZnO nanopowder after each thermal treatment.

The TEM bright field image, figure 4A, of ZnO nanoparticles as obtained from n-buthanol reveals that the powder is composed from polyhedral elongated shaped particles, with an average particle size of approximately 18 nm. The nanopowder is well dispersed with no amorphous phase present.
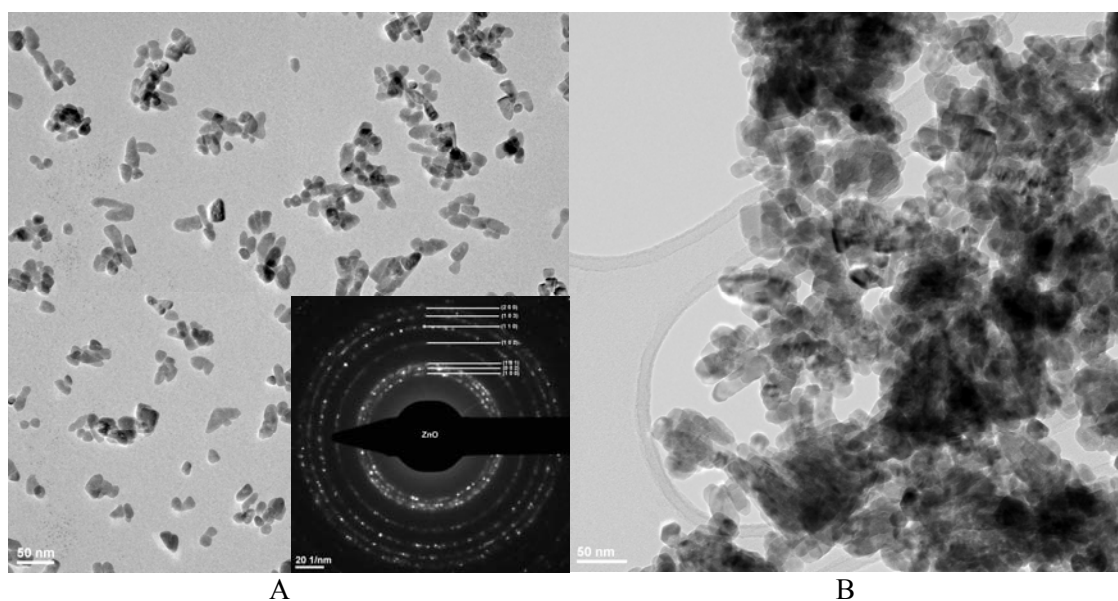
Fig. 4. (A) TEM images of ZnO nanoparticles as obtained from n-buthanol; inset- SAED pattern of planes of hexagonal structure ZnO [ASTM 80-0075]; (B) TEM images of ZnO nanoparticles after annealing 2hrs at 900ºC.

From the selected area diffraction pattern obtained on ZnO nanopowder, we can state that the only phase identified is the crystalline hexagonal form of ZnO [ASTM 80-0075]. Moreover, the SAED image of ZnO nanoparticles confirms the Miller indices of characteristic crystalline structures identified by XRD (inset of figure 4A).

The TEM bright field image, figure 4B, of the ZnO powder after annealing process at 900ºC for 2 hours reveals the tendency of the ZnO nanoparticles to form soft agglomerates. The sintering, together with the coalescence of the nanoparticles can explain the variation observed in the XRD pattern.

The luminescence spectra, figure 5, show that the as-synthesized samples have a wurtzite structure, with a weaker NBE emission, and two blue-green emissions, one centred at 457 nm (with a shoulder at 448 nm) and a second at 482 nm. The weak green emission is present around 514 nm.

The weak UV emission at 400 nm is assigned to the free exciton emission from the wide band gap of ZnO (NBE). This peak is shifted to 389 nm upon increasing the annealing temperature to 500ºC, and 382nm for 900ºC. This blue shift is opposed to what was observed elsewhere [34]. It has also been reported that the NBE peak of 389.2 nm was observed for ZnO with O_i defects [35].

In our previous work [36, 37] we have reported that ZnO samples obtained by pyrosol and sol gel methods implying temperatures of 700ºC and 400ºC respectively present luminescent properties in the usual range.

High intensity of the green and blue-green luminescence versus NBE are reported in literature whenever the luminescence spectra is recorded on powders as obtained, without further treatments (simple annealing or annealing in presence of reducing atmosphere) [38, 39].

It has been reported that the sub-band-gap emission in ZnO depends on the morphology of the nanostructures. [40-42]. A blue-green emission at 453 nm and a green emission at around 557 nm as found in literature for nest like nanoparticles [41] and emissions at 421 nm, 482 nm, and 532 nm for nanocones [42]. For as nanorods, most of the spectral weight is in the sub-bandgap, centred on 625 nm [38]. The intensity of the visible emission peak also correlates with the particle size [44].
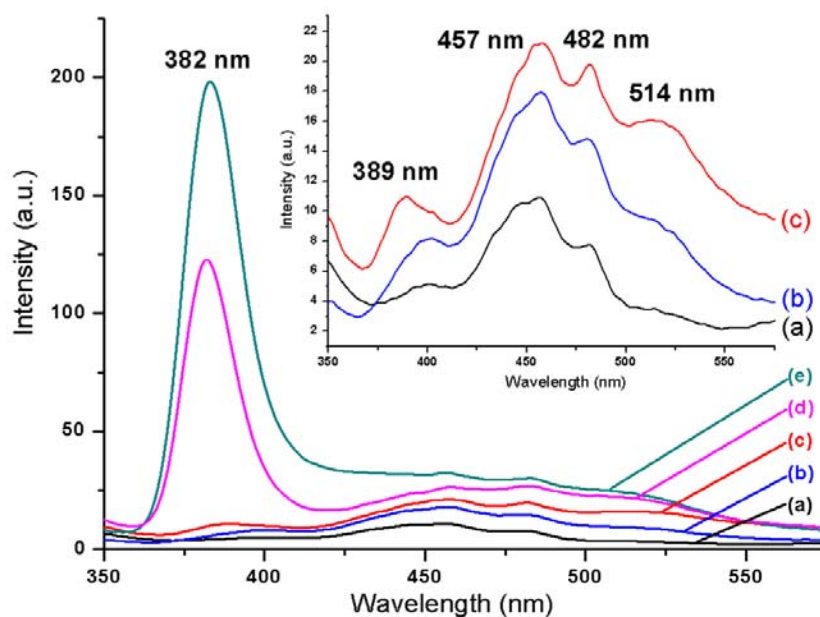
Fig. 5. Photoluminescence spectra of ZnO nanopowder obtained for different thermal treatment temperatures: as obtained (a); 300ºC (b); 500ºC (c); 700ºC (d); 900ºC (e); inset – detail of the PL spectra for a), b) and c) samples.

The calculated energy levels of the intrinsic defects in ZnO are reported, and the calculated energy levels of V_{Zn}, Zn_i, V_O, O_i, and O_{Zn} are 3.06, 2.9, 1.62, 2.28, and 2.38 eV, respectively [45].

The emission in the blue-green range (bands at 448, 457, 482, and 514 nm) are defect-related emissions. The exact cause of them is still controversial. The luminescence bands at 448, 457 and 482 nm are believed to be caused by the transition from the level of the ionized oxygen vacancies to the valence band [40] or can be attributed to band-edge free excitons and bound excitons, respectively [46, 47]. The 482 nm band is relatively common for semiconductor oxides like MIn_2O_4 (M = Ca, Sr, Ba) or SnO_2 [48, 49] confirming that it is caused by the oxygen related defects [50, 51].

The 514 nm emission is even more controversial. In some reports it is attributed to surface anion vacancies [26, 52], by a mechanism that involves the tunnelling of surface-bound electrons through pre-existing trapped holes in oxygen vacancies (Vo•) resulting in the creation of recombination centres (Vo••) for visible emission. Mo et al [43] explicate this in terms of defect levels associated with oxygen vacancies and zinc interstices. These defects are most probably on the nanocrystals surfaces, causing faster and more effective trapping of the photo-generated holes at the surface sites.

X. Fang et al. [53] and Hseih et al [26] manage to alter the intensity ratio of the NBE to the green emission by altering the flowing atmosphere in the furnace. They explain it in terms of V_O number decrease as increasing partial pressure of oxygen.

Other reports [24, 54] indicate that green emission has a direct correlation with the increasing of density of O_i and O_{Zn} defects and not with V_O.

M.K. Lee and H.F. Tu [55] presented mix results regarding green emission with no clear pattern of variation. This nonlinear variation of the green emission intensity was attributed by authors to the elimination of water molecules from the nanoparticles surface.

In fact by a simple literature survey one can understand that the variation of the luminescence properties depend not only to the post synthesis treatment (temperature, time, atmosphere), but also to the synthesis method itself.

In our experiment, we manage to increase both UV and blue-green emissions, at different rates, altering the intensities ratio UV_PL/Vis_PL from 0.4 to 5. The NBE emission band intensity was improved by a simple 2 hours annealing at 900ºC. As annealing temperature is increasing to 700ºC and further to 900ºC respectively, there is a major increase in the UV emission, the intensity increasing in total more than 40 times.

The blue-green emission intensity also increases but at a moderate rate of 3 times only, which is consistent with the results from the FTIR spectra. This behaviour can be correlated with two parallel processes: increasing of the crystalline order in the nanoparticles, which leads to fewer surface defects [56, 57] and the formation of O_{Zn}, V_{Zn}, O_i defects by dissociation from oxygen-rich states that is responsible for the stronger blue-green band [54, 55].

Our results are in good agreement with those reported elsewhere [53]. This tuning of emission intensity can be helpful in obtaining high efficiency ZnO emitters, in the desired spectrum region.
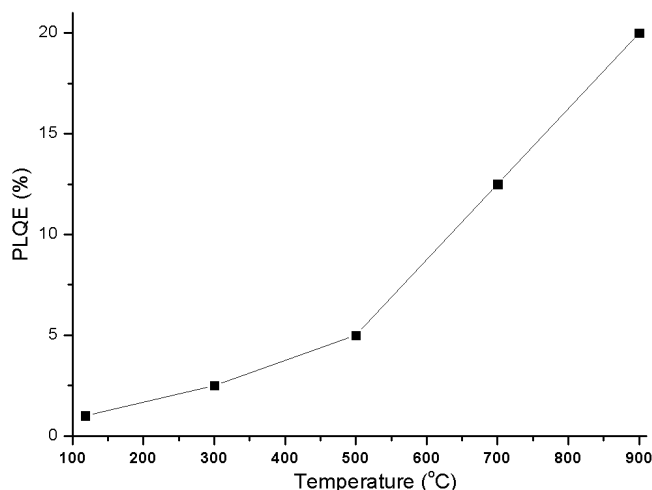

Fig. 6. The PLQE variation vs. annealing temperature

A maximum photoluminescence quantum efficiency (PLQE) of 20.1% was obtained for the ZnO nanocrystals annealed at 900°C (figure 6). The PLQE was determined by comparing the wavelength-integrated intensity of the ZnO nanocrystals with that of a standard quinine sulphate using the following equation [58]:

$$Q = Q_R \cdot (I \cdot A_R \cdot \eta^2)/(I_R \cdot A \cdot \eta_R^2) \tag{I}$$

where Q is the PLQE of nanocrystals, Q_R is the PLQE of the reference (quinine sulphate), I and I_R are the integrated intensities, A and A_R are the absorbance at 325 nm, and η and η_R are the refractive indices of the nanocrystals and the reference, respectively.

The PLQE of the ZnO nanocrystals increases with the annealing temperature, quite sharply after 500°C. This increase is due to the major contribution of the high intensity NBE band.

Mishra et al [59] reported that the temperature increase after 600°C has no effect on the excitonic emission. However, we present here evidence that thermal treatment enhanced the PLQE to an exceptionally high value. With increasing heat-treatment temperature, the decrease in some defect type (V_O, Zn_i) concentration should strengthen the excitonic luminescence, and a rise in PLQE of the excitonic emission has been observed.

The electronic spectra recorded for the ZnO powders, as obtained and annealed, are presented in figure 7A. The highest UV absorption (0.96) is presented in as obtained ZnO powder. The intensity of UV absorption band is decreasing slightly with increasing the annealing temperature, to 0.83. The UV maximum also suffers a hypsochromic shift from 365 nm to 358 nm as the annealing temperature is increasing.

The fundamental absorption refers to the optical transition of electrons from the valence band to conduction band and can be used to determine the nature and values of optical band gap of the nanoparticles [60, 61]. For analysis purposes the diffuse reflectance, R, of the sample can be related to the Kubelka-Munk function F(R) by the relation $F(R)=(1-R)^2/2R$, [62]. To determine the band-gap energies (Eg) for the ZnO nanoparticles, a plot of the square of the modified Kubelka-Munk function vs. the energy is presented in the figure 7B. This yields the direct band gap energy. Adopting the method proposed by Cao et al., [63] the band-gap energies (Eg) for the ZnO

nanoparticles are determined to be 3.20 - 3.25 eV, by the extrapolation to $[F(R) \cdot hv]^2 = 0$. The calculated band gap values for ZnO are in good agreement with the literature [64, 65].
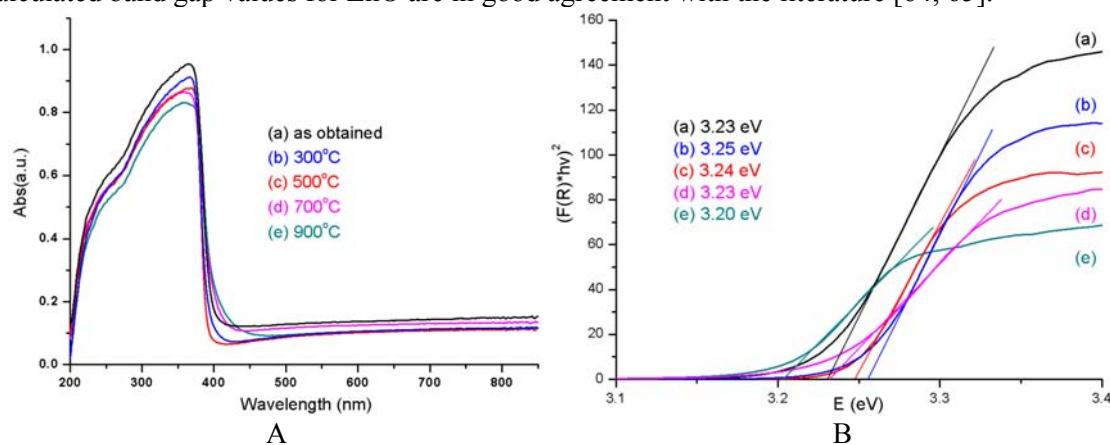

Fig. 7. Diffuse reflectance spectra (A) and plot of the transformed Kubelka-Munk function vs. the energy (B) for the ZnO powder: as obtained (a) and annealed at 300°C (b); 500°C (c); 700°C (d); 900°C (e)

We observed an initial increase in the band gap value as the ZnO powder is annealed at 300°C, probably due to elimination of some electronic levels belonging to hydroxo species. After that initial step, there is an inverse correlation between annealing temperature and bang gap value. As the temperature increase from 300 to 900°C the band gap value is decreasing from 3.25eV to 3.20eV. This weak dependence is similar with the values from other reports [21, 66] This was attributed to the formation of O_i and O_{Zn} surface defects, which introduce new electronic levels inside band gap [54].

Also Vishwas et al [67] have reported before that NBE emission intensity will be enhanced with the decreasing value of the band gap energy, which is similar with our findings.

4. Conclusions

A synthetic method for obtaining nanocrystalline ZnO particles in n-buthanol has been presented. The colloid process was carried out at refluxing temperature (118°C), with the solutions free from alkali ions. TEM and XRD data sustain the formation of a single phase, monodisperse crystalline ZnO. The ZnO particles were chemically pure in terms of cation impurities and exhibited blue-green photoluminescence. We found that the annealing temperature dramatically influences the photoluminescence of the ZnO nanoparticles. We found that NBE emission shifts from 389 to 382 as the annealing temperature increase to 900°C and in same time the intensity increase over 40 times. In the same time, the blue green emission increases only 3 times. This makes it possible to selectively enhance the NBE emission performance to suit various applications.

The experimental data sustain the hypothesis that blue green emission is not related to Vo defects but rather to O_i, V_{Zn} and O_{Zn} type defects. The slightly asymmetric shape of NBE emission band indicates the existence of an increasing number of O_i defects. This is in good agreement with the decreasing of the band gap value, calculated from UV-Vis spectra. The exceptionally high PLQE obtained for the samples annealed at 900°C indicate that defects responsible for quenching the NBE emission are removed.

References

[1] C.I. Covaliu, T. Mălăeru, G. Georgescu, O. Oprea, L. Alexandrescu, I. Jitaru - Digest Journal of Nanomaterials and Biostructures, **6**(4), 1491 (2011).

[2] D. Ficai, A. Ficai, B. S. Vasile, M. Ficai, O. Oprea, C. Guran, E. Andronescu - Digest Journal of Nanomaterials and Biostructures, 6(3), 943 (2011).

[3] C.I. Covaliu, L. C. Chioaru, L. Crăciun, O. Oprea, I. Jitaru, Optoelectron. Adv. Mater. – Rapid Commun. **5**(10), 1097 (2011).

[4] A. Ianculescu, F. Prihor Gheorghiu, P. Postolache, O. Oprea, L.Mitoseriu - Journal of Alloys and Compounds **504**(2), 420 (2010).

[5] K.S. Weißenrieder, J. Muller, Thin Solid Films. **300**, 30 (1997).

[6] F. Vaja (Dumitru), C. Comanescu, O. Oprea, D. Ficai, C. Guran - Revista de Chimie – **63**(7), 722 (2012).

[7] M. A. Behnajady, N. Modirshahla, E. Ghazalian, Dig J Nanomater Bios. **6**, 467 (2011).

[8] J. Neamtu, C.M. Teodorescu, G. Georgescu, J. Ferre, T. Malaeru, I. Jitaru, *Structural and Magneto-Optical Properties of Co-doped ZnO Thin Films Prepared by Sol-Gel Method*, NSTI NANOTECH 2008.,TECHNICAL, vol.1, 2008, pp. 238-241, ISBN**:** 978-1-4200-8503-7

[9] A. Radu, S. Iftimie, V. Ghenescu, C. Besleaga, V.A. Antohe, G. Bratina, L. Ion, S. Craciun, M. Girtan, S. Antohe, Dig J Nanomater Bios. **6**, 1141 (2011).

[10] A. Gupta, H.S. Bhatti, D. Kumar, N.K. Verma, R.P. Tandon, Dig J Nanomater Bios. **1**, 1 (2006).

[11] S. Ghosh, V. Sih, W. H. Lau, D. D. Awschalam, S.-Y. Bae, S. Wang, S.Vaidya, G. Chapline, Appl. Phys. Lett. **86**, 232507 (2005).

[12] K. Ogata, K. Koike, S. Sasa, M. Inoue, M. Yano, Appl Surf Sci **254**, 7708 (2008).

[13] S. Major, S. Kumar, M. Bhatnagar, K.L. Chopra, Appl. Phys. Lett. **49**, 394 (1986).

[14] A.F. Kohan, G. Ceder, D. Morgan, Chris G. Van de Walle, Phys. Rev. B. **61**, 15019 (2000).

[15] Z.R. Tian, J.A. Voigt, J. Liu, B. Mckenzie, M.J. Mcdermott, M.A. Rodriguez, H. Konishi, H.F. Xu, Nat. Mater. **2**, 821 (2003).

[16] C.H. Bae, S.M. Park, S.C. Park, J.S. Ha, Nanotechnology. **17**, 381 (2006).

[17] T. Sekiguchi, N. Ohashi, Y. Terada, Japanese Journal of Applied Physics Part **2**(36) L289 (1997).

[18] X. Liu, X. Wu, H. Cao, R. P. H. Chang, Journal of Applied Physics. **95**, 3141 (2004).

[19] W. S. Shi, O. Agyeman, C. N. Xu, Journal of Applied Physics. **91**, 5640 (2002).

[20] D. Wang, N. Reynolds, Condensed Matter Physics. (2012) Article ID 950354, doi:10.5402/2012/950354.

[21] Jianguo Lv, Wanbing Gong, Kai Huang, Jianbo Zhu, Fanming Meng, Xueping Song, Zhaoqi Sun, Superlattices and Microstructures. **50**, 98 (2011).

[22] B. Lin, Z. Fu, Y. Jia, G. Liao, Journal of the Electrochemical Society. **148**, G110 (2001).

[23] M. Anpo, Y. Kubokawa, Journal of Physical Chemistry. **88**, 5556 (1984).

[24] Sung-Sik Chang, Journal of the Korean Ceramic Society. **48**, 251 (2011).

[25] M. Rajalakshmi, S. Sohila, S. Ramya, R. Divakar, Chanchal Ghosh, S. Kalavathi, Optical Materials. **34**, 1241 (2012).

[26] P.T. Hsieh, Y.C. Chen, K.S. Kao, C.M. Wang, Appl. Phys. A **90**. 317 (2008).

[27] S. H. Bae, S. Y. Lee, H. Y. Kim, S. Im, Optical Materials. **17**, 327 (2001).

[28] Y. G. Wang, S. P. Lau, H. W. Lee, Journal of Applied Physics. **94**, 354 (2003).

[29] O. Oprea, E. Andronescu, B.S. Vasile, G. Voicu, C. Covaliu, Dig J Nanomater Bios. **6**, 1393 (2011).

[30] A. Kaschner, U. Haboeck, M. Strassburg, M. Strassburg, G. Kaczmarczyk, A. Hoffmann, C. Thomsen, A. Zeuner, H.R. Alves, D.M. Hofmann, B.K. Meyer, Appl. Phys. Lett. **80**, 1909 (2002).

[31] G. Xiong, U. Pal, J.G. Serrano, K.B. Ucer, R.T. Williams, Phys. Stat. Sol. (C) 3, 3577 (2006).

[32] A. Djelloul, M-S. Aida, J. Bougdira, Journal of Luminescence **130**, 2113 (2010).

[33] S. Golshahi, S.M. Rozati, Dig J Nanomater Bios. **6**, 413 (2011).

[34] Ming-Kwei Lee, Hwai-Fu Tu, Journal of Applied Physics **101**, 126103 (2007).

[35] F. Wen, W. Li, J.-H. Moon, J. H. Kim, Solid State Commun., **135**, 34 (2005).

[36] O Oprea, O. R. Vasile, G. Voicu, L. Craciun, E. Andronescu - Dig J Nanomater Bios. **7**(4), 1757 (2012).

[37] O.R. Vasile, E. Andronescu, C. Ghitulica, B.S. Vasile, O. Oprea, E. Vasile, R. Trusca – Journal of Nanoparticle Research, (2012) 14:1269, DOI: 10.1007/s11051-012-1269-7

[38] J.W.P. Hsu, D.R.Tallant, R.L. Simpson, N.A. Missert, R.G. Copeland, Applied Physics Letters **88**, 252103 (2006).

[39] Sh. U. Yuldashev, Sung Woo Choi, Tae Won Kang, Journal of the Korean Physical Society. **42**, S216 (2003).

[40] W.M. Kwok, A.B. Djurisic, Y.H. Leung, W.K. Chan, D.L. Phillips, Appl. Phys. Lett. **87**, 223111 (2005).

[41] Li Yan, Feng Hui-yun, Zhang Nan, Liu Chuan-sheng, Trans. Nonferrous Met. Soc. China 20, 119 (2010).

[42] Zhang, D. H., Wang, Q. P. and Xue, Z. Y. Appl. Surf. Sci. **207**, 20 (2003)

[43] Mo C M, Li Y H, Lin Y S, Zhang Y and Zhang P L J. Appl. Phys. **83**, 4389 (1998).

[44] M. Wang, E.K. Na, J.S. Kim, E.J. Kim, S.H. Hahn, C. Park, K.K. Koo, Mater. Lett. **61**, 4094 (2007).

[45] B. X. Lin, Z. X. Fu, Y. B. Jia, Appl. Phys. Lett., **79**, 943 (2001).

[46] Li Yan, Feng Hui-yun, Zhang Nan, Liu Chuan-Sheng, Trans. Nonferrous Met. Soc. China. **20**, 119 (2010).

[47] J. Liqianga, Q. Yichuna, W. Baiqia, L. Shudana, J. Baojianga, Y. Libina, F. Weia, F. Honggang, S. Jiazhong, Sol. Energy Mater. Sol. Cells. **90**, 1773 (2006).

[48] D. Gingasu, O. Oprea, I. Mindru, D. C. Culita, L. Patron, Dig J Nanomater Bios. **6**, 1215 (2011).

[49] A.M. Ungureanu, I. Jitaru, Bull Sci UPB, B Series, in press

[50] Yunqing Zhu, Yiqing Chen, Xinhua Zhang, European Journal of Chemistry. **2**, 8 (2011).

[51] Nurul Syahidah Sabri, Ahmad Kamal Yahya, Mahesh Kumar Talari, Journal of Luminescence **132**, 1735 (2012).

[52] Y. Du, M.S. Zhang, J. Hong, Y. Shen, Q. Chen, Z. Yin, Appl. Phys. A **76**, 171 (2003).

[53] X.S. Fang, Y. Bando, U.K. Gautam, T. Zhai, H. Zeng, X. Xu, M. Liao, D. Golberg, Critical Reviews in Solid State and Materials Sciences. **34**, 190 (2009).

[54] X. M. Fan, J. S. Lian, Qing Jiang, ZuoWan Zhou, J Mater Sci. **42**, 2678 (2007).

[55] Ming-Kwei Lee, Hwai-Fu Tu, Jpn. J. Appl. Phys. **47**, 980 (2008).

[56] X.S. Fang, C.H. Ye, L.D. Zhang, Y. Li, Z.D. Xiao, Chem. Lett., **34**, 436 (2005).

[57] S. Cho, J. Ma, Y. Kim, Y. Sun, G. K. L. Wong, and J. B. Ketterson:Appl. Phys. Lett. **75**, 2761 (1999)

[58] J.R. Lackowicz, Principles of Fluorescence Spectroscopy, Kluwer Academic/Plenum, New York, 1999, pp.53.

[59] A.K. Mishra, S.K. Chaudhuri, S. Mukherjee, A. Priyam, A. Saha, D. Das, J. Appl. Phys. **102**, 103514 (2007).

[60] S.M. Rozati, E.Shadmani, Dig J Nanomater Bios. **6**, 365 (2011).

[61] S. Singh, H. Kaur, D. Pathak, R.K. Bedi, Dig J Nanomater Bios. **6**, 689 (2011).

[62] G. Kortum, Reflectance Spectroscopy, Springer-Verlag, New York, 1969.

[63] G. Cao, L.K. Rabenberg, C.M. Nunn, T.E. Mallouk, Chem. Mater. **3**, 149 (1991).

[64] P. Muthukumara, T.M. Selvakumarib, S. Ganesan, Dig J Nanomater Bios. **5**, 635 (2010).

[65] F.I. Ezema, U.O.A. Nwankwo, Dig J Nanomater Bios. **5**, 981 (2010).

[66] J.H. Cai, G. Ni, G. He, Z.Y. Wu, Physics Letters A. **372**, 4104 (2008).

[67] M. Vishwas, K. Narasimha Rao, K.V. Arjuna Gowda, R.P.S. Chakradhar, Spectrochimica Acta Part A. **77**, 330 (2010).